A differential linear perturbation method for apparent I.P. calculations.

Loke[1], M.H, Wilkinson[2], P.B. and Frankcombe[3], K.

[1] Retired, Penang, Malaysia. drmhloke@gmail.com (Associate Editor, Journal of Applied Geophysics)
[2] British Geological Survey, Nottingham, U.K. pbw@bgs.ac.uk
[3] ExploreGeo, Perth, Australia. kim@exploregeo.com.au

Statement
This is a non-peer-reviewed preprint submitted to EarthArXiv..

Date : 22nd August 2026

ABSTRACT

3-D induced polarization (I.P.) surveys are widely used in exploration of minerals particularly those that contain conductive minerals sulfides that frequently occur in areas with complex geology. The linear perturbation method is frequently used to calculate the apparent resistivity and I.P. values. This method treats the I.P. effect as a linear change of a base conductivity model. The apparent I.P. value is calculated by dividing the difference in the resistivity potentials between the base and perturbed conductivity models with the base model potential. This can lead to significant numerical roundoff errors if the difference in the potentials is much smaller than the base model potential. This occurs if there is large range variation in the model resistivity values and the arrays used have a large range of geometric factors. The use of double-precision calculations or a complex conductivity model greatly reduces the roundoff errors. However, these methods significantly increases the computer memory needed by more than 70% and the calculation time by more than 50%. A new differential linear perturbation method is proposed that calculates the change in the potentials directly (instead of from the difference between the two potential values) that avoids the roundoff error problems. It increases the computer memory by 3% and calculation time by 9%. It enables the calculation of more accurate apparent I.P. values for finite-element models with millions of nodes using a PC.

1 Introduction

Induced polarization (I.P.) surveys are widely used in the exploration of mineral deposits particularly those containing conductive metallic sulfides either as the main orebody or accessory minerals. The mineral deposits usually occur in areas with complex geology that have a large range of resistivity values which can only be accurately mapped by using 3-D I.P. surveys. In order to cover a large area (frequently with rugged topography) with a limited number of survey lines, the offset pole-dipole (White et al., 2001; Collins and White, 2007) or dipole-dipole (Frankcombe, 2015; McGill and Farquhar-Smith, 2015) arrays are frequently used. The arrays usually have very large dipole lengths (50 to 200 m) with the current dipole offset from the potential dipole. This results in electrode arrays with very high geometric factors, and consequently very low potentials measured at the potential dipole electrodes. Interpretation of the field data requires a 3-D resistivity and I.P. inversion program (White et al., 2001; Loke et al., 2025). The forward modelling routine used to calculate the apparent resistivity and I.P. values is a central component of a 3-D inversion computer program. The use of different methods to calculate the apparent I.P. values is examined in this paper.

2 Computation of apparent I.P. values

The linear-perturbation method described by Oldenburg and Li (1994) is widely used in the calculation of apparent I.P. values for the interpretation of data from field surveys. This method treats the I.P. conductivity model (σ_{IP}) as a linear perturbation of a base DC conductivity model (σ_{DC}). The effect of the intrinsic I.P. value (m) is to change the effective conductivity (σ_{IP}) of the material.

$$\sigma_{IP} = \sigma_{DC} - m\sigma_{DC} \quad (1)$$

It is assumed that the change in the conductivity is linearly proportional to the material I.P. value m. The apparent I.P. value m_a measured by an electrode array is then calculated from potentials obtained over a medium with the original DC conductivity model (ϕ_{DC}) and that obtained for the perturbed conductivity model (ϕ_{IP}) using the following equation.

$$m_a = [\phi_{IP} - \phi_{DC}]/\phi_{DC} \quad (2)$$

or

$$m_a = \Delta\phi/\phi_{DC}, \text{ where } \Delta\phi = \phi_{IP} - \phi_{DC}. \text{ or } \phi_{IP} = \phi_{DC} + \Delta\phi. \quad (3)$$

The apparent I.P. value is calculated as the ratio of the difference in the potentials ($\Delta\phi$) and the DC potential ϕ_{DC}. The potentials calculated by the finite-element method with a computer have a finite accuracy. Numerical roundoff errors occur due to the floating-point numerical

operations (addition, subtraction, multiplication, division) carried out to obtain the potential values for the conductivity model. For an apparent I.P. anomaly of 0.1 mV/V, the difference in the potentials $\Delta\phi$ is ten thousand times smaller the DC potential ϕ_{DC}. Small numerical roundoff errors can have a significant effect on the final calculated apparent I.P. value m_a. A modification to the linear perturbation method is described in the following section that greatly reduces the effect of the roundoff errors.

The results are also compared to the apparent I.P. values calculated using a different mathematical model proposed by Kenma et al. (2000). The nonlinear complex conductivity method treats the conductivity as a complex quantity with real and imaginary components. The I.P. value appears in the complex component. The complex conductivity is given by the following equation.

$$\sigma = \sigma_{DC} - i\, m_i \sigma_{DC} \tag{4}$$

A complex potential with real and imaginary components is then calculated.

$$\phi = \phi_r + i\, \phi_i \tag{5}$$

The apparent chargeability is calculated from the ratio of the imaginary (ϕ_i) and real (ϕ_r) potentials. An advantage of this method is that it can be used for spectral I.P. models where the I.P. effect changes with frequency (Loke et al., 2006). Here it is used as an independent method to check the apparent I.P. values calculated by the linear perturbation method.

The finite-element method (Silvester and Ferrari, 1990) is used to calculate the potentials as it can easily incorporate topography. This method gives the following capacitance matrix equation that is solved to calculate the potentials.

$$\mathbf{C\Phi = s} \tag{6}$$

C is the capacitance matrix that contains the model conductivity values and positions of the nodes in the finite-element mesh. $\boldsymbol{\phi}$ is the potential vector to be calculated and **s** is the current vector. **C** is a symmetric positive-definite matrix that is very sparse (Loke et al., 2018; Loke et al., 2022). Direct methods to solve this equation can be thousands of time faster than iterative methods (Loke, 1994; Oldenburg et al., 2013) for finite-element problems with many sources and receivers (electrodes). Large 3-D ERT surveys can have more than 1 million electrode positions (Unrau, 2019) and the finite-element mesh used might have several million nodes (Loke et al., 2025). Most I.P. surveys are carried out by small to medium sized companies with limited computational resources (usually a PC or workstation) that have limited memory and processing power. The numerical method used must be able to calculate the potentials for very large meshes and many electrode positions using the limited computer facilities available within a reasonable time

A widely used direct method to solve the matrix equation (6) is the Cholesky decomposition method for sparse matrices (George and Liu, 1981; Loke, 1994; Karypis and Kumar, 1998; Schenk et al., 2001; Davis, 2006). This method has two main steps. First the capacitance matrix **C** (which is symmetric and positive definite) is factored into a lower triangular matrix **L**.

$$\mathbf{C = LL^T} \tag{7}$$

The potential values are then calculated using a two-step algorithm. The following triangular matrix system is first solved to obtain a temporary vector **y**.

$$\mathbf{Ly = s}, \text{where } \mathbf{y = L^T\Phi} \tag{8}$$

This is followed by the backwards substitution step that solves the following matrix equation to obtain the potential vector $\boldsymbol{\Phi}$.

$$\mathbf{L^T\Phi = y} \tag{9}$$

The same triangular matrix **L** is used to calculate the potentials for different electrode positions, so the factorisation step only needs to be carried out once. The original capacitance matrix **C** has less than $10n$ non-zero values for a 3-D finite-element mesh (n is the number of nodes). The factorised matrix **L** has a much larger number of non-zero values, in the order of *n.log(n)*, using modern sparse matrix techniques (Davies, 2006). The matrix is stored in two sets of

arrays; several 64-bit integer arrays (as the number of non-zero values in **L** can exceed two billion for very large meshes) that contains the sparse block structure of **L**, and floating point arrays (32-bit for single-precision, 64-bit for double precision) that contain the numerical values. Complex floating point arrays are used for **C**, **L**, **s** and **y** when the complex conductivity method is used.

The Pardiso sparse matrix solver (Schenk et al., 2001) function in the Intel MKL library (Intel, 2018) is used for the numerical calculations. This software library is optimised for PCs using the Intel x86 CPUs. A PC with an Intel 12900K CPU with 16 cores and 128GB RAM is used for the calculations.

3 A new differential linear perturbation method

The weakness of the standard linear perturbation method comes from finding a small change in the potentials $\Delta\phi$ from the difference between two much larger values ϕ_{IP} and ϕ_{DC} in equation (3). Solving the capacitance matrix (equations (7) to (9)) involves billions of floating point operations for large finite-element meshes. The round-off error due to the finite precision of the floating point numbers used (32-bit for single-precision arithmetic) adds up with each operation. One way to solve this problem is to calculate the difference $\Delta\phi$ directly (instead of from the difference between larger two values). The potentials due to the resistivity model, ϕ_{DC}, is calculated using the following equation.

$$\mathbf{C_{DC}\Phi_{DC}} = \mathbf{s} \tag{10}$$

$\mathbf{C_{DC}}$ is the capacitance matrix calculated from the model conductivity values σ_{DC} and finite-element mesh geometry. It is independent of the potential vector $\mathbf{\Phi_{DC}}$ and current vector **s**. To calculate the potentials $\mathbf{\Phi_{IP}}$ due to the perturbed conductivity model the following equation is used.

$$\mathbf{C_{IP}\Phi_{IP}} = \mathbf{s} \tag{11}$$

$\mathbf{C_{IP}}$ is the capacitance matrix for perturbed conductivity model. The current vector **s** is the same in equations (10) and (11). Thus, they can then be combined as follows.

$$\mathbf{C_{IP}\Phi_{IP}} = \mathbf{C_{DC}\Phi_{DC}} \tag{12}$$

The perturbed conductivity σ_{IP} can be written as the result of the DC conductivity σ_{DC} minus the change in the conductivity $\Delta\sigma$.

$$\sigma_{IP} = \sigma_{DC} - m\sigma_{DC} = \sigma_{DC} - \Delta\sigma, \text{ where } \Delta\sigma = m\sigma_{DC}. \tag{13}$$

The change in the conductivity changes the capacitance matrix from $\mathbf{C_{DC}}$ to $\mathbf{C_{IP}}$.

$$\mathbf{C_{IP}} = \mathbf{C_{DC}} + \Delta\mathbf{C}, \quad \Delta\mathbf{C} = \mathbf{C_{IP}} - \mathbf{C_{DC}} \tag{14}$$

$\Delta\mathbf{C}$ is the change in the capacitance matrix. Next $\mathbf{\Phi_{IP}}$ in equation (12) is replaced by equation (3).

$$\mathbf{C_{IP}}(\mathbf{\Phi_{DC}} + \Delta\mathbf{\Phi}) = \mathbf{C_{DC}\Phi_{DC}} \tag{15}$$

$\Delta\mathbf{\Phi}$ is the change in the potential vector which is needed. Expanding this equation gives

$$\mathbf{C_{IP}\Phi_{DC}} + \mathbf{C_{IP}}\Delta\mathbf{\Phi} = \mathbf{C_{DC}\Phi_{DC}} \, . \tag{16}$$

Rearranging the terms gives the following equation.

$$\mathbf{C_{IP}}\Delta\mathbf{\Phi} = (\mathbf{C_{DC}} - \mathbf{C_{IP}})\,\mathbf{\Phi_{DC}}$$

This can be simplified by using equation (14).

$$\mathbf{C_{IP}}\Delta\mathbf{\Phi} = \Delta\mathbf{C}\,\mathbf{\Phi_{DC}}$$

The above equation can be written as

$$\mathbf{C_{IP}}\Delta\mathbf{\Phi} = \Delta\mathbf{s}, \text{ where } \Delta\mathbf{s} = \Delta\mathbf{C}\,\mathbf{\Phi_{DC}} \tag{17}$$

$\Delta\mathbf{s}$ is a pseudo current vector created by multiplying the change in the capacitance matrix $\Delta\mathbf{C}$ with the DC potentials vector $\mathbf{\Phi_{DC}}$. The DC potentials vector $\mathbf{\Phi_{DC}}$ is calculated in the first step of the linear perturbation method. The current source **s** vector for an electrode, such as in equation (6), usually only has a single or few non-zero values (Loke et al., 2018, 2022). However, $\Delta\mathbf{s}$ is a full vector with non-zero values at all the nodes of the finite-element mesh since $\Delta\mathbf{C}$ has at least one non-zero value in each row and $\mathbf{\Phi_{DC}}$ is a full vector. Equation (17)

has the same form as equation (6) so it can also be solved using the Cholesky decomposition method to determine the change in the potential values $\Delta\mathbf{\Phi}$ directly. The apparent I.P. values are then calculate as follows.

$$m_a = \Delta\phi / \phi_{DC} \tag{18}$$

The change in the potential $\Delta\phi$ is calculated directly by solving the capacitance matrix equation (17) instead of from the difference between two larger potential values which avoids the numerical roundoff error problem.

4 Comparison of the apparent resistivity and I.P. values for a synthetic model

Figure 1a shows a 3-D synthetic model with high resistivity and I.P. contrasts. The resistivity values range from 50 to 2000 Ω.m, while the I.P. values range from 2 to 60 mV/V. The target is a rectangular body with higher I.P. values (and lower resistivity values) within a two-layer medium. The test model has the electrodes arranged in a 102 by 101 rectangular grid with a 10 m spacing. The finite-element mesh used has 4625208 nodes. A test was made with the inline dipole-dipole array with a dipole length 'a' of 10 m and dipole separation factors 'n' of 1 to 14. The apparent resistivity and I.P. values are measured along parallel lines aligned in the x-direction. A comparison is made between the apparent resistivity and I.P. values calculated using 32-bit single-precision and 64-bit double-precision floating point arrays for the capacitance matrix **C**, the current (**s**) and potential ($\mathbf{\Phi}$) vectors. Since the resistivity and I.P. structures are symmetrical, and the inline dipole-dipole is a symmetrical array, the anomalies should also show a symmetrical pattern.

Figures 1b and 1c shows the horizontal apparent resistivity pseudosections obtained using the single-precision and double-precision linear perturbation methods for 'n' values of 6, 8, 10, 12 and 14. There are no significant differences between the apparent resistivity values calculated by the two methods. The region with the low resistivity structure shows a prominent symmetrical low apparent resistivity anomaly in both sets of pseudosections.

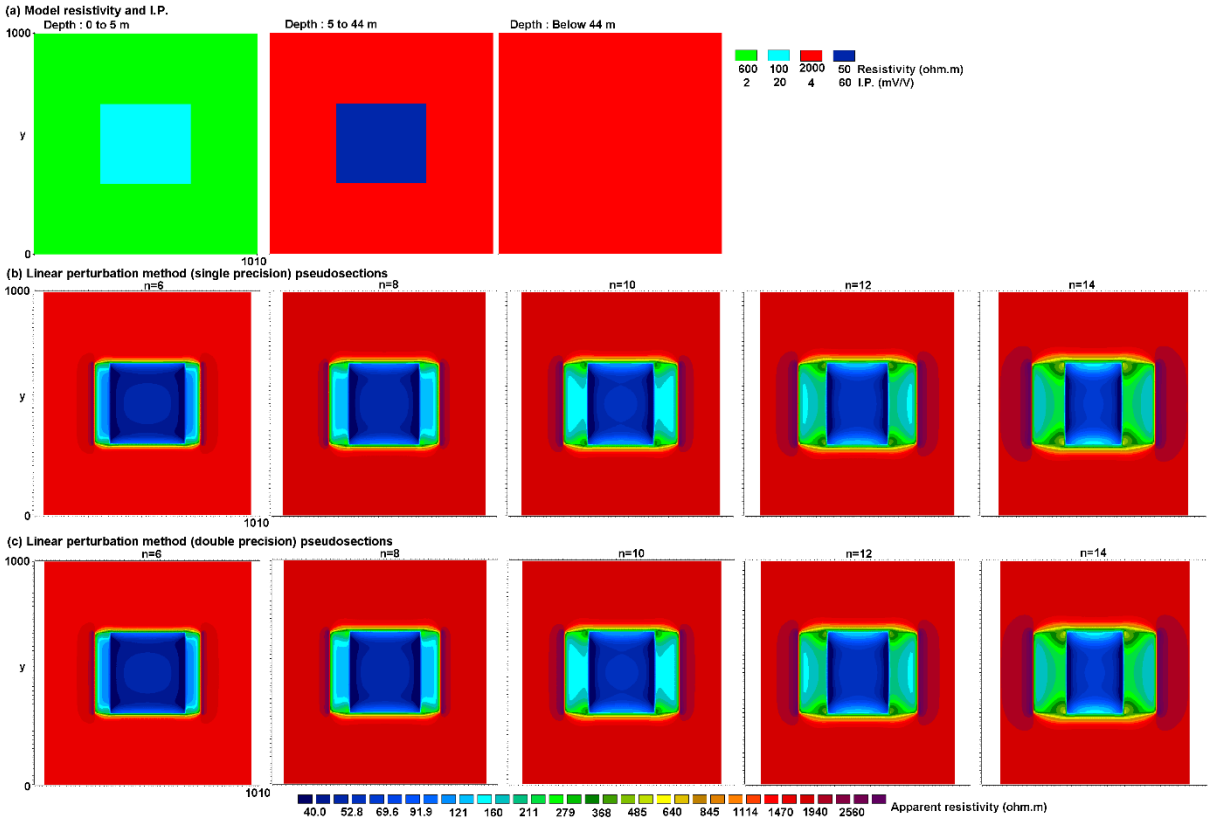

Figure 1. (a) Model resistivity and I.P. values. Apparent resistivity pseudosections calculated using the (b) single-precision and (b) double-precision linear perturbation methods.

Figure 2 shows the horizontal apparent I.P pseudosections obtained using four different methods. Figure 3 shows profile plots for a survey line in the x-direction across the middle of the model. The double-precision linear perturbation method (Figure 2b) shows the expected smooth symmetrical contour pattern. However, the single-precision linear perturbation method shows irregular contours for 'n' values greater than 6 (Figure 2a). This is more clearly shown in the profile plots in Figure 3a. The apparent I.P. values (red dots) calculated by the single-precision method closely follows those calculated by the double-precision method (black line) for 'n=6'. Small deviations are visible for 'n=8', that becomes increasingly more prominent for 'n=10' and 'n=12', and very obvious for 'n=14' (Figure 3a). This is due random 'noise' caused by numerical roundoff errors in the calculation of the potential values. The geometric factor for the dipole-dipole array is approximately proportional to n^3. The geometric factor for 'n=14' is 10 times higher than for 'n=6'. The potential values are reduced by the same factor as the array 'n' value increases. This makes the effect of the numerical roundoff errors in the calculation of the apparent I.P. values greater for arrays with higher geometric factors.

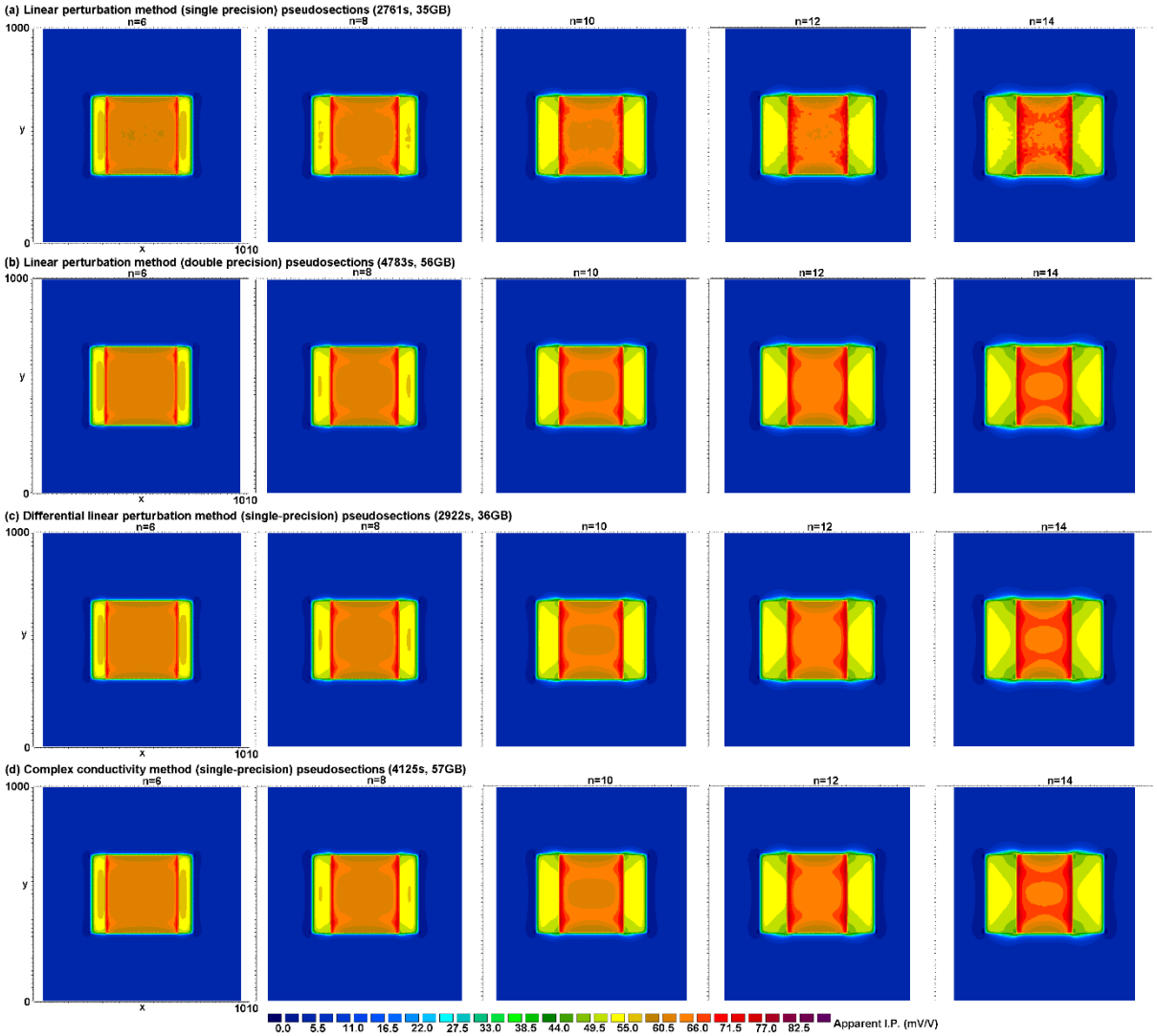

Figure 2. Horizontal apparent I.P. pseudosections calculated using the (a) single-precision linear perturbation, (b) double-precision linear perturbation, (c) differential linear perturbation and (d) complex conductivity methods. The computer time and memory required by the different methods are also shown.

An error of 0.1% in the $\phi(\sigma_{DC})$ and $\phi(\sigma_{IP})$ values in equation 2 will cause an error of 1 mV/V in the apparent I.P. value. The linear perturbation method using double-precision numerical arrays has much lower roundoff errors. However, this causes a significant increase in the computer calculation time and memory required (Table 1). The double-precision method requires double the computer memory space to store the numerical values of the **L** matrix compared to the single-precision method (the memory required by the integer arrays containing the structure of the sparse matrices remain the same). For this model, the increase in the computer memory required is about 21 GB. The total computer memory required is 56Gb compared to 35Gb for the single-precision method (Table 1), so it cannot used if the PC has only 48GB RAM. It might be possible to overcome the larger computer memory required by using other techniques such as out-of-core storage but they would be much slower. In this example, the double-precision method is about 80% slower than the single-precision method and requires 60% more memory. The larger computer memory and longer calculation time required can be a practical limitation for very large finite-element meshes with more than 10 million nodes for PCs.

There are no significant differences between the apparent I.P. values calculated using the double-precision linear perturbation (Figure 3b) and the single-precision differential linear perturbation method (Figure 2c and 3b). The computer memory required by the differential method (36GB) is marginally higher than the single-precision linear perturbation method (35GB) but much lower than the double-precision linear perturbation method (56GB). The maximum difference with the values calculated using the double-precision method is 0.28 mV/V, compared to 6.33 mV/V for the standard single-precision linear perturbation method (Table 1). The RMS difference for all arrays for with 'n' values ranging from 1 to 14 is 0.01 mV/V which is not significant as most field surveys probably have noise levels above 1 mV/V (particularly in mineral exploration surveys where large dipole spacings of 50 to 100 meters are widely used). The increase in calculation time (9%) and memory (3%) compared the standard single-precision linear perturbation method are small, while the apparent I.P. values are comparable to those obtained with the double-precision method. It eliminates the problem of the less accurate apparent I.P. values obtained by the single-precision linear perturbation method at the cost of a slightly higher computer calculation time and memory.

Figure 2d shows the pseudosections obtained using the single-precision complex conductivity method. It shows the smooth symmetrical contour pattern similar to the double-precision linear perturbation method (Figure 2b). However, it was observed that there are small systematic differences compared to double-precision method (particularly for the higher 'n' values in areas with high I.P. values). This is probably due to the difference in the mathematical approach used by the two methods. The difference only appears for arrays with very high geometric factors. The maximum difference is 1.27 mV/V, while the RMS difference is 0.10 mV/V which is not significant compared to the noise level in most fields surveys. The computer memory required (57GB) is significantly higher than the differential linear perturbation method (36GB) and it is about 40% slower (Table 1). The complex method requires twice as much computer memory for the floating point arrays.

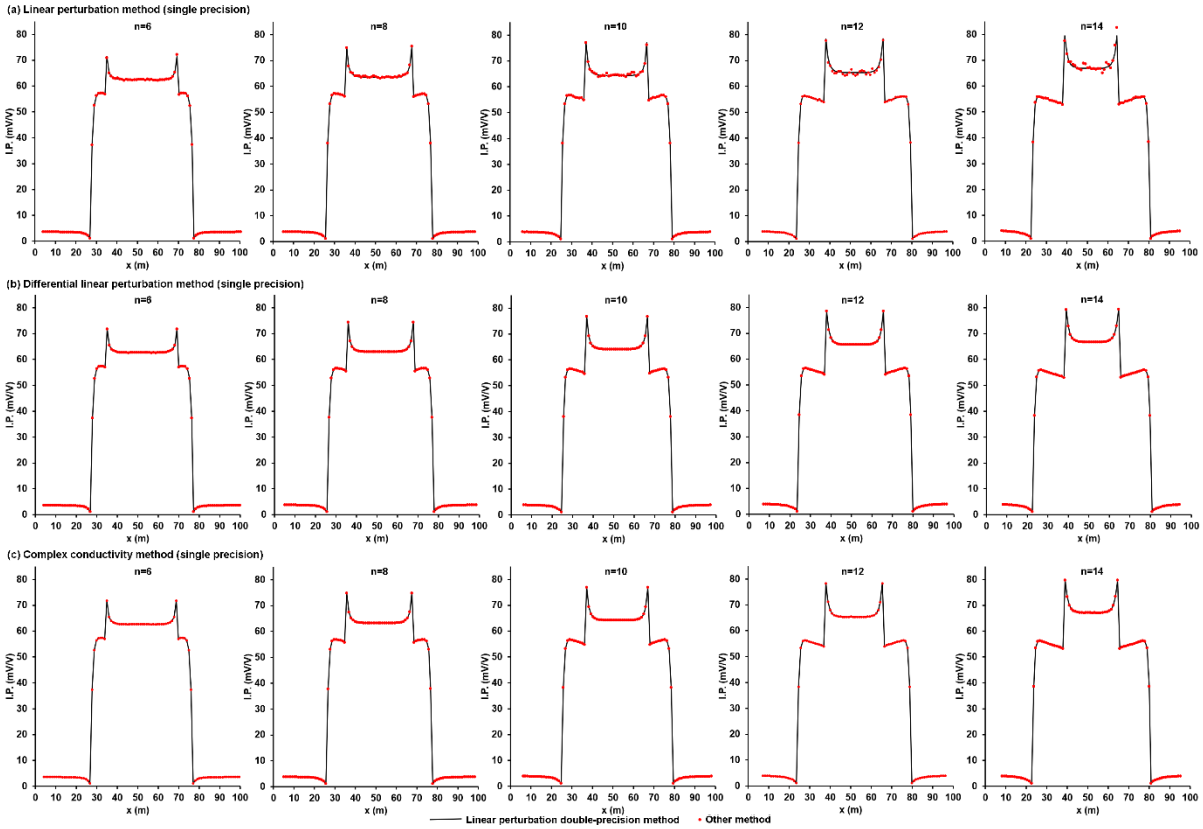

Figure 3. Apparent I.P. profiles in the x-direction across the middle of the model calculated using the different methods for dipole-dipole array 'n' values of 6, 8, 10, 12 and 14.

Table 1**.** Calculation time and memory required by the different methods. The differences in the apparent I.P. values (in mV/V) calculated by the other methods compared to the double-precision linear perturbation (L.P.) method are listed. The RAM shown in brackets is the net memory used by the program after subtracting that used by the Windows operating system.

Methods	Time (s)	Memory (GB)	Max. diff. (mV/V)	RMS diff. (mV/V)
L. P. (single)	2671	35 (27)	6.33	0.18
L.P. (double)	4783	56 (48)	-	-
Differential L.P. (single)	2922	36 (28)	0.28	0.01
Complex (single)	4125	57 (49)	1.27	0.10

5 Model with a lower resistivity contrast

The model in Figure 1a has a large maximum resistivity contrast where the resistivity of the rectangular block (50 ohm.m) is 40 times lower than the surrounding medium (2000 ohm.m). Another test was carried out using a resistivity model with a lower maximum resistivity contrast of 5 but with the same model I.P. values (Figure 4a). The 'noise' in the single-precision linear perturbation I.P. pseudosections is significantly reduced (Figure 4b). There are some slight asymmetries in the I.P. pseudosections for ‘n’ values above 10 compared to the double-precision method (Figure 4c), but the differences are much less severe compared to Figure 2. The differences between the single-precision linear perturbation and the double-precision profiles are barely visible in the profile plot (Figure 4d). The maximum difference in the apparent I.P. values is 0.53 mV/V which is much smaller compared to 6.33 mV/V for the model with larger resistivity contrasts. The high resistivity contrasts in the first model (Figure

1a) and the large geometric factors for the higher ‘n’ values cause the more severe round-off errors in the apparent I.P. values calculated using the single-precision linear perturbation method. Large changes in the model resistivity values result in similar large changes in the potential values. The apparent I.P. value for the dipole-dipole array is calculated by adding and subtracting the potential values from four different current-potential electrodes pairs. This leads to more severe roundoff errors if one or more of the potential values are large compared to the others.

6 Conclusions

The standard single-precision linear perturbation method can result in significant errors in the calculated apparent I.P. values for electrode arrays with large geometric factors and models with large resistivity and I.P. contrasts due to numerical roundoff errors. Such a situation sometimes occur in large mineral exploration surveys where the inline or offset dipole-dipole array with large electrode spacings are used in areas with large resistivity and I.P. contrasts. The differential linear perturbation method significantly reduces the errors by calculating the change in the potentials directly instead of from the difference between two resistivity potential values. The reduction in the computer memory required enables the calculations for I.P. models with very large meshes (possibly with tens of millions of nodes) where the memory required by the slower double-precision and complex conductivity methods exceeds the available computer memory. The increase in the computer calculation time and memory required is less than 10% compared to the standard single-precision linear-perturbation method. This is particularly important for the inversion of huge I.P. data sets with a large number of electrode positions using a large finite-element mesh with millions of nodes where the forward modeling routine is used repeatedly within an inversion program.

Acknowledgements

Wilkinson publish with the permission of the Executive Director of the British Geological Survey.

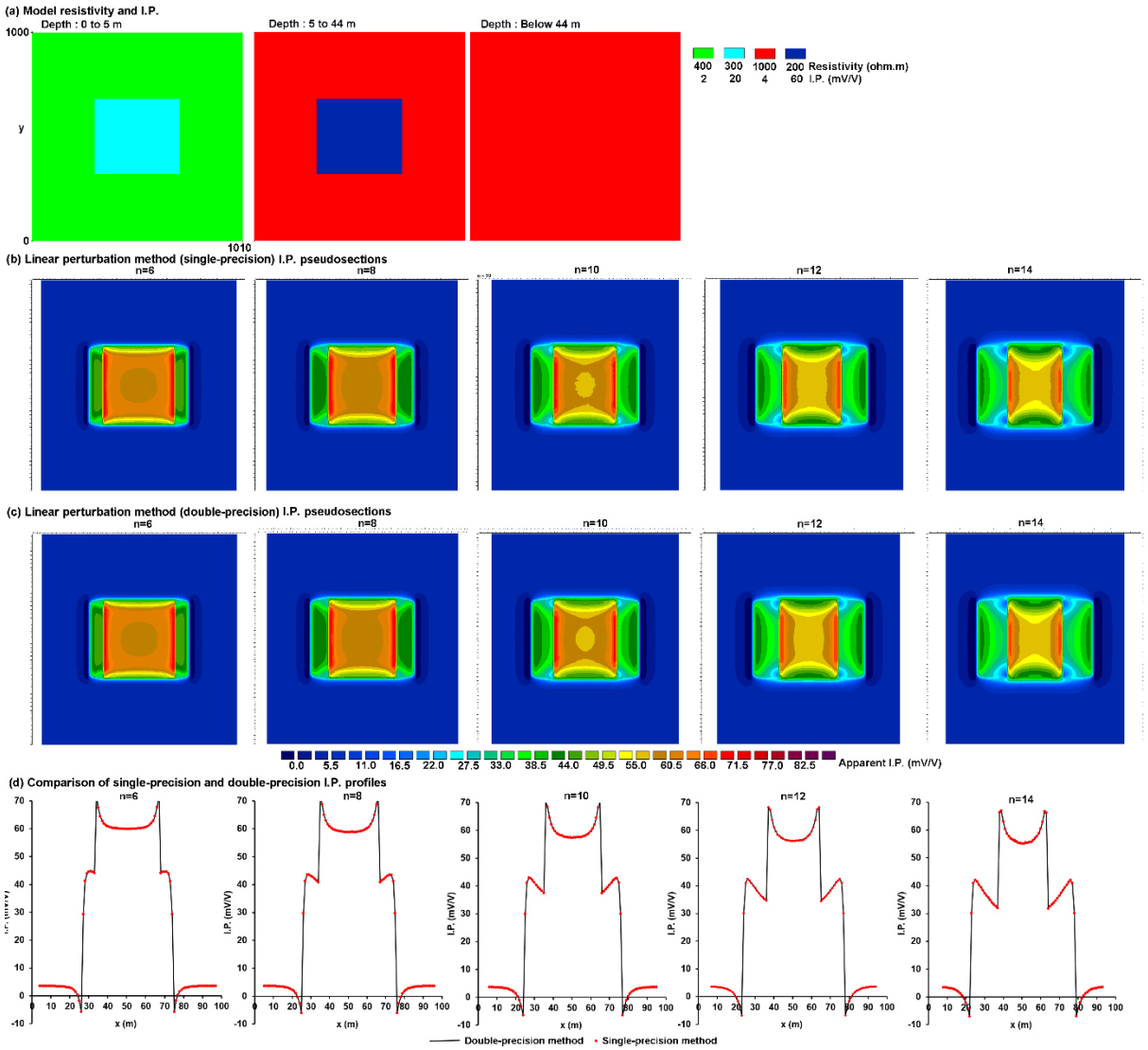

Figure 4. (a) Model with lower resistivity contrast. Apparent I.P. pseudosections calculated using the (b) single-precision and (c) double-precision linear perturbation methods. (d) Apparent I.P. profiles in the x-direction across the middle of the model calculated using the single-precision and double-precision methods for the dipole-dipole array with 'n' values of 6, 8, 10, 12 and 14.

References

Collins, S. and White, R.M.S., 2007. Six years experience with Offset pole-dipole and other 3D IP arrays. What have we learnt? ASEG Extended Abstracts, 2007:1, 1-4, DOI: 10.1071/ASEG2007ab023

Davis, T.A., 2006. Direct methods for sparse linear system. Society for Industrial and Applied Mathematics.

Frankcombe, K., 2015. Offset dipole-dipole array. ASEG-PESA 2015, Perth, Australia.

George, A. and Liu, J.W.H., 1981. Computer solution of large sparse positive definite systems. Prentice-Hall, Inc., NJ.

Intel, 2018. Intel® Math Kernel Library 2018 (Intel® MKL). Intel Corporation.

Karypis, G. and Kumar, V., 1998. A fast and high quality multilevel scheme for partitioning irregular graphs. SIAM J. Sci. Comput., 20(1), 359-392.

Kenma, A., Binley, A., Ramirez, A. and Daily, W., 2000. Complex resistivity tomography for environmental applications. Chemical Engineering Journal, 77, 11-18.

Loke, M.H., 1994. The inversion of two-dimensional resistivity data. Unpubl. PhD thesis, Un. of Birmingham.

Loke, M.H., Chambers, J.E. and Ogilvy, R. D., 2006. Inversion of 2-D spectral induced polarization imaging data. Geophysical Prospecting. 54, 287-301.

Loke, M.H., Wilkinson, P.B., Chambers, J. E. and Meldrum, P.I., 2018. Rapid inversion of data from 2-D resistivity surveys with electrodes displacements. Geophysical Prospecting, 66, 579-594.

Loke, M.H., Wilkinson, P.B., Kuras, O., Meldrum, P.I. and Rucker, D.F., 2022. The use of a semi-structured finite-element mesh in 3-D resistivity inversion. Geophysical Prospecting, 70, 1580-1601.

Loke, M.H., Frankcombe, K. and Unrau,, T., 2025. Challenges in the inversion of large 3-D resistivity and I.P. data sets. AEGC conference, 8-11 September 2025, Perth, WA, Australia.

McGill, D. and Farquhar-Smith, D., 2015. A comparison of 3D DCIP data acquisition methods. ASEG-PESA 2015, Perth, Australia.

Oldenburg D.W and Li Y. 1994. Inversion of induced polarization data. Geophysics, 59, 1327-1341.

Oldenburg, D.W., Haber, E., Shekhtman, R., 2013. Three dimensional inversion of multisource time domain electromagnetic data. Geophysics 78, E47-E57.

Schenk, O., Gärtner, K., Fichtnera, W., Stricker, A., 2001. PARDISO: a high-performance serial and parallel sparse linear solver in semiconductor device simulation. Future Generation Computer Systems, 18, 69–78.

Unrau, T., 2019. Towed Capacitively Coupled Resistivity Systems in Arctic Exploration - Advances in Equipment Design and Handling of Very Large Resistivity Surveys. AGU 100 Fall Meeting, San Francisco, 9-13 Dec. 2019, NS22A-07.

White, R.M.S., Collins, S., Denne, R., Hee, R. and Brown, P., 2001. A new survey design for 3D IP modelling at Copper Hill. Exploration Geophysics, 32, 152-155.